ISSN 0234-5366

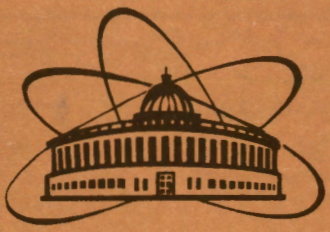

ОБЪЕДИНЕННЫЙ
ИНСТИТУТ
ЯДЕРНЫХ
ИССЛЕДОВАНИЙ

JOINT INSTITUTE
FOR NUCLEAR
RESEARCH

4[55]-92

КРАТКИЕ СООБЩЕНИЯ ОИЯИ

JINR RAPID COMMUNICATIONS

ДУБНА

Объединенный институт ядерных исследований
Joint Institute for Nuclear Research

№4 [55] -92

КРАТКИЕ СООБЩЕНИЯ ОИЯИ
JINR RAPID COMMUNICATIONS

сборник
collection

Дубна 1992

ОГЛАВЛЕНИЕ
CONTENTS

УДК 539.126

$K^{\pm}$ BACKWARD PRODUCTION IN pA INTERACTIONS AT 15—65 GeV

O.P.Gavrishchuk, V.F.Peresedov, L.S.Zolin

The invariant cross sections of the yield of K^+ and K^- mesons are measured at an angle of 159° on 6 nuclear targets (Be, C, Al, Ti, Mo, W) at an incident proton energy from 15 to 65 GeV. The momentum spectra of kaons are measured by the method of thin target on an internal beam of the Serpukhov proton accelerator (IHEP). The kaon spectra are investigated in a momentum interval from 350 to 800 MeV/c what corresponds to the range of the light cone variable $\alpha = 1 + 1.9$. The A-dependence of the K^+ and K^- cross sections is essentually different: $\sigma_k(W)/\sigma_k(Be)$ is equal to ≈ 10 for K^+ and about 2 for K^-. The ratio R of the K^+ and K^- yields demonstrates a weak dependence on α, but it grows substantially with increasing A: $R(Be) \approx 10$ and $R(W) \approx 50$. In the frame of the Fluctuon Fragmentation Model, $R(\alpha, A)$ can be connected with the redistribution of valent and sea quarks in the nucleus (in particular, with the reinforcement of the quark sea in fluctuons).

The investigation has been performed at the Laboratory of High Energies, JINR.

Выход $K^{\pm}$ назад в pA-взаимодействиях при 15—65 ГэВ

Гаврищук О.П.;Переседов В.Ф., Золин Л.С.

Измерены инвариантные сечения рождения K^+- и K^--мезонов под углом 159° на шести ядерных мишенях (Be, C, Al, Ti, Mo, W) при энергии падающих протонов — от 15 до 65 ГэВ. Импульсные спектры каонов измерены с использованием метода тонких внутренних мишеней на внутреннем пучке протонного синхротрона ИФВЭ (Серпухов). Спектры каонов исследованы в импульсном интервале от 350 до 800 МэВ/с, что соответствует интервалу значений переменной светового фронта $\alpha = 1-1.9$. А-зависимость сечений для K^+ и K^- существенно различна: $\sigma_K(W)/\sigma_K(Be)$ равно 10 для K^+ и около 2 для K^-. Отношение R выходов K^+ и K^- демонстрирует слабую зависимость от α, но существенно растет с увеличением А: $R(Be) = 10$ и $R(W) = 50$. В рамках модели фрагментации флуктуонов $R(\alpha, A)$ может быть связано с перераспределением валентных и морских кварков в ядрах (в частности, с усилением кваркового моря во флуктуонах).

Работа выполнена в Лаборатории высоких энергий ОИЯИ.

The production of high momentum mesons ($q \geq 0.5$ GeV/c) at angles close to 180° in nuclear fragmentation under the influence of high energy beams is not an ordinary phenomenon because it cannot be explained within the framework of the simplified model of the nucleus with quasi free nucleons.

One of the approaches used to explain this phenomenon arises from the hypothesis of interaction of a projectile with a density fluctuation of nuclear matter-fluctuon. This formation can be presented either as a multinucleon cluster [1] or as multiquark configuration [2,3] or as a few-nucleon correlation [4]. Constituent quarks of the fluctuon form a generalized multiquark system, and one of its quarks-partons can carry a momentum which is in the limit equal to the total momentum of all nucleons involved in such formation. We call hadrons, products of fluctuon fragmentation, «cumulative» according to [5].

Using the model based on the hypothesis of the presence of multiquark configurations in nuclei, a successful quantitative reproduction of the spectra of cumulative pions has been made [6]. There has been no detailed comparison of model predictions with experimental data for kaons and antiprotons until recently. On the one hand, this was connected with insufficient data for K^-- and $\bar{p}$-production at $\theta \approx 180°$ and, on the other hand, cross section calculation for «sea» cumulative particles ($K^-, \bar{p}$) not containing valence quarks of the nucleus requires grounded notions about properties of the quark sea in nuclei.

In our experiment [7,8] we have measured differential production cross sections for positive and negative kaons at an angle of 159° (lab. system) in proton-nucleus collisions at a proton energy from 15 to 65 GeV. The experiment was carried out on an internal beam of the IHEP proton synchrotron (Serpukhov). Six types of targets were used: Be, C, Al, Ti, Mo and W. The targets were prepared in the form of thin wires ($\phi < 100\,\mu$) to provide a multiple circulation of the internal proton beam across the target. This made it possible to take data on an increasing magnetic field of the accelerator and to have long runs without obstacles for the other users. The latter is important because of very small cross sections for backward cumulative particle production which is about 1 nb (at $q_k \approx 0.8$ GeV/c) in the case of K^-. The momentum spectra of kaons were measured from 0.35 to 0.8 GeV/c which corresponds to the light cone variable $\alpha = (E_k - q_k \cos\theta_k)/m_N$ from 1 to 1.9. The value of minimum target mass, x_m, measured in units of nucleon mass, m_N, is often used as a scaling variable to discribe cumulative data ($x_m = 1$ corresponds to the kinematic limit for production on free nucleon at rest). The variable x_m coincides with α and the Bjorken variable x at $E \to \infty$; x_m exceeds α by 5—10% at our energies (15—65 GeV). The rise of the invariant cross sections for kaons is insignificant over an energy range from 15 to 65 GeV: it is on the average about 20% as in the case of pions [8]. Further on we use the

Table 1. Invariant cross section $(E/A)d\sigma/d^3q$ (mb GeV^{-2}c^{3}sr^{-1}/nucleon) for the reaction $p + A \to K^+(159°)$ at $\overline{E}_p = 40$ GeV

q (GeV/c)	T (GeV)	Be	C	Al
0.350	0.111	(0.124±0.010)E-1	(0.198±0.039)E-1	(0.430±0.172)E-1
0.400	0.142	(0.640±0.045)E-2	(0.820±0.132)E-2	(0.280±0.084)E-1
0.450	0.174	(0.292±0.020)E-2	(0.390±0.062)E-2	(0.125±0.025)E-1
0.500	0.209	(0.105±0.010)E-2	(0.225±0.038)E-2	(0.680±0.340)E-2
0.550	0.245	(0.710±0.085)E-3	(0.660±0.185)E-3	(0.195±0.135)E-2
0.600	0.283	(0.262±0.016)E-3	(0.450±0.027)E-3	
0.650	0.322	(0.970±0.078)E-4	(0.181±0.015)E-3	(0.367±0.026)E-3
0.700	0.363	(0.436±0.048)E-4	(0.572±0.057)E-4	(0.172±0.016)E-3
0.750	0.404	(0.151±0.027)E-4	(0.197±0.032)E-4	(0.710±0.092)E-4
0.800	0.446		(0.750±0.180)E-5	(0.260±0.065)E-4

q	x_R	Ti	Mo	W
0.350	1.039	(0.560±0.168)E-1	(0.930±0.240)E-1	0.115±0.014
0.400	1.129	(0.300±0.087)E-1	(0.360±0.075)E-1	(0.525±0.058)E-1
0.450	1.217	(0.175±0.049)E-1	(0.173±0.075)E-1	(0.248±0.042)E-1
0.500	1.309	(0.660±0.250)E-2	(0.990±0.280)E-2	(0.910±0.136)E-2
0.550	1.404	(0.240±0.096)E-2	(0.330±0.155)E-2	(0.400±0.080)E-2
0.600	1.498	(0.172±0.012)E-2	(0.189±0.010)E-2	(0.206±0.012)E-2
0.650	1.596	(0.710±0.057)E-3	(0.750±0.045)E-3	(0.110±0.007)E-2
0.700	1.696	(0.263±0.031)E-3	(0.364±0.026)E-3	(0.447±0.027)E-3
0.750	1.796	(0.107±0.017)E-3	(0.114±0.012)E-3	(0.180±0.015)E-3
0.800	1.897	(0.290±0.087)E-4	(0.440±0.097)E-4	(0.880±0.088)E-4

cross sections averaged over beam energy, E_p, with a mean value of $\overline{E}_p = 40$ GeV.

The normalized invariant cross sections of K^+- and K^--production, $\rho_k = (E_k/A)d\sigma/d^3q_k$, are presented in tables 1 and 2 and in figs.1 and 2. The indicated errors are statistical, the absolute normalization error is estimated to be 15%. The invariant cross sections can be approximated by the exponents of the variables α and T (kinetic energy of kaons): $\rho_k = C'\exp(-\alpha/\alpha_0)$ and $\rho_k = C\exp(-T/T_0)$. The dependences of the parameters α_0 and T_0 on mass number A are shown in fig.3.

Table 2. Invariant cross section $(E/A)d\sigma/d^3q$ (mb $GeV^{-2}c^3\,sr^{-1}$/nucleous) for the reaction $p + A \to K^-(159°)$ at $\overline{E}_p = 40$ GeV.

q (GeV/c)	α	Be	C	Al
0.350	0.992	(0.116±0.023)E-2		(0.250±0.150)E-2
0.400	1.077	(0.700±0.105)E-3	(0.820±0.115)E-3	(0.500±0.500)E-3
0.450	1.160	(0.353±0.049)E-3	(0.400±0.048)E-3	(0.102±0.061)E-2
0.500	1.247	(0.118±0.029)E-3	(0.190±0.023)E-3	
0.550	1.336	(0.550±0.250)E-4	(0.112±0.022)E-3	(0.185±0.130)E-3
0.600	1.425	(0.860±0.390)E-5	(0.213±0.055)E-4	(0.330±0.110)E-4
0.650	1.517	(0.870±0.310)E-5	(0.107±0.029)E-4	(0.128±0.045)E-4
0.700	1.610	(0.322±0.162)E-5	(0.590±0.114)E-5	(0.710±0.284)E-5
0.750	1.704	(0.135±0.095)E-5	(0.354±0.114)E-5	(0.450±0.200)E-5
0.800	1.798		(0.830±0.580)E-6	

q	x_m	Ti	Mo	W
0.350	1.058	(0.195±0.116)E-2	(0.220±0.100)E-2	(0.215±0.034)E-2
0.400	1.147	(0.740±0.520)E-3	(0.133±0.040)E-2	(0.108±0.013)E-2
0.450	1.238	(0.960±0.480)E-3	(0.450±0.148)E-3	(0.500±0.100)E-3
0.500	1.331	(0.410±0.246)E-3	(0.260±0.091)E-3	(0.182±0.045)E-3
0.550	1.426	(0.150±0.150)E-3	(0.980±0.390)E-4	(0.760±0.230)E-4
0.600	1.522	(0.670±0.200)E-4	(0.240±0.091)E-4	(0.500±0.080)E-4
0.650	1.620	(0.167±0.075)E-4	(0.175±0.058)E-4	(0.157±0.031)E-4
0.700	1.721	(0.700±0.490)E-5	(0.990±0.400)E-5	(0.113±0.025)E-4
0.750	1.822	(0.880±0.530)E-5	(0.300±0.180)E-5	(0.380±0.113)E-5
0.800	1.924	(0.450±0.450)E-5	(0.310±0.190)E-5	(0.270±0.135)E-5

The slope of the spectra decreases with increasing A for K^+ and K^-, i.e. the «temperature» of the spectra, T_0, increases. However, the A-dependence of K^+ and K^- production is substantially different: as is seen from fig.4, the ratio of the invariant cross sections for W and Be, ρ_W/ρ_{Be}, is equal to 10 for K^+ and about 2 for K^-. As a rule the A-dependence of particle production is characterized by the power of mass number: $E_k d\sigma_{K^\pm}/d^3q_k \sim A^{\alpha\pm}$. The dependence of $\alpha^\pm$ on q_k is shown in fig.5; in the case of K^+ the A-dependence differs substantially ($\alpha^+ = 1.6$) from the volume type dependence, A^1.

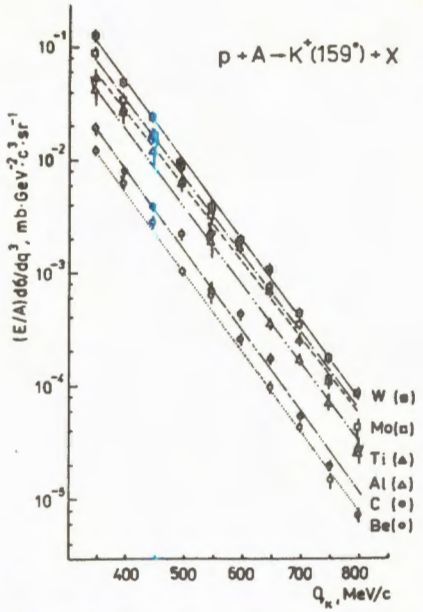

Fig.1. Invariant cross sections for the reaction $p + A \to K^+(159^\circ) + X$

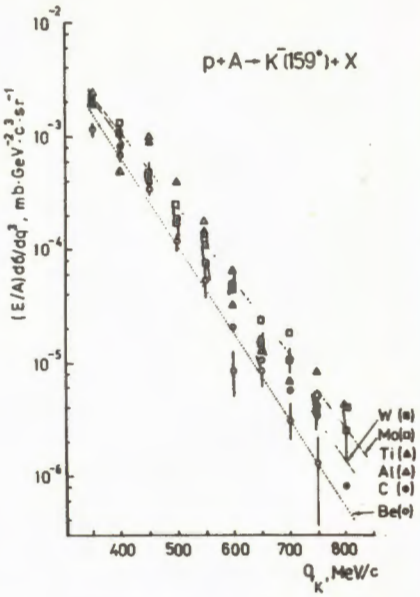

Fig.2. Invariant cross sections for the reaction $p + A \to K^-(159^\circ) + X$, errors (statistical) are shown only for Be and W

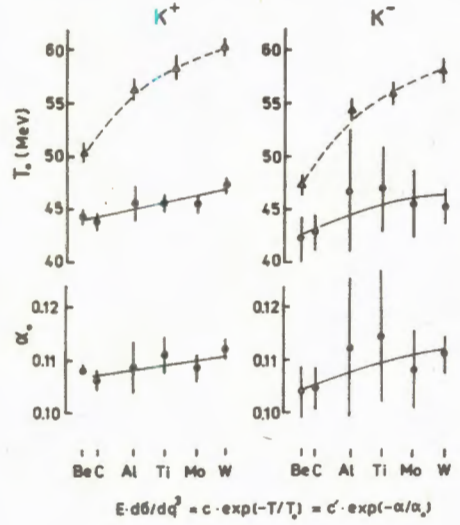

Fig.3. Dependence of the slope parameters, α_0 and T_0, on A for the spectra of $K^+(\bullet)$ and $K^-(\circ)$ at $E_p = 40$ GeV and $\theta_k = 159^\circ$. ▲, △ – data for $E_p = 10$ GeV and $\theta_k = 119^\circ$ [9].

It is shown [11] that main features of the EMC effect can be explaned if the nucleus is considered as a relativistic quantum system in which baryon number is conserved but the number of particles is not fixed. Due to vacuum polarization, the nucleus is not only the system of A nucleons

but also the sea of particles-antiparticles which carries some part of nucleus momentum. As a consequence, an additional «collective» sea of $q\bar{q}$ — pairs as hard as the valence quark distribution should exist in the nucleus along with the seas of quark-antiquarks and gluons in valence nucleons. This «collective» sea determines the spectrum of antiquarks at high x and also the spectrum of «sea» cumulative particles $(K^-, \bar{p})$. Proceeding from the assumtion of the concentration of the additional quark sea in fluctuons, the authors of the Fluctuon Fragmentation Model (FFM) [12] have calculated the momentum spectra of π^+ and K^+ in the reaction $p + d \to \pi^+, K^+(180°)$. The reproduction of the experimental data was quite satisfactory for the fluctuon component in the deuteron (free parameter) equal to 3.6%. The ratio π^+/K^+ calculated in this model is compared with our data for the Be nucleus (fig.6), the ratio and its x_m-dependences coincide well although the multiscattering effect in nuclei is not taken into account in this comparison.

The ratio of the K^+- and K^- yields must reflect a difference in the x-distribution of valence and sea quarks: this ratio should have a slight momentum dependence at $x > 0.5$ if the distribution of antiquarks in the «collective» sea is as hard as that of valence

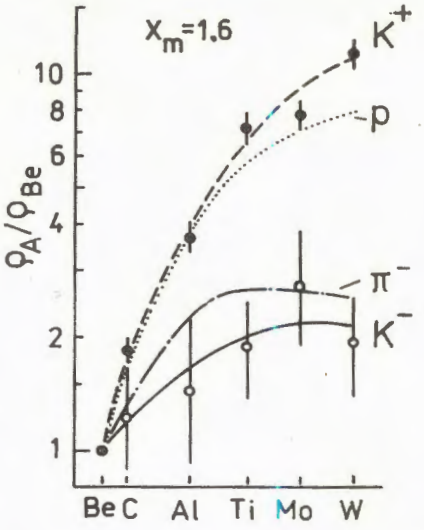

Fig.4. A-dependence of hadron production in the reaction $p + A \to h(159°) + X$ at $E_p = 40$ GeV. The dependences for π and p are presented using the data from [8,10]

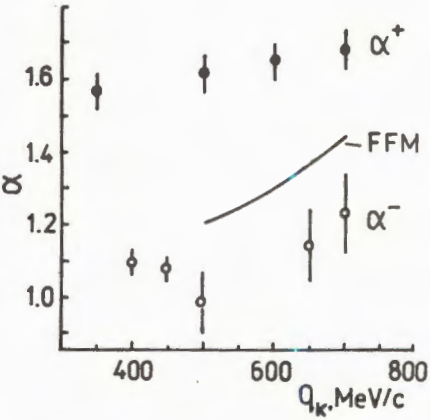

Fig.5. Momentum dependence of the power of mass number, $\alpha^{\pm}$, in case of presentation of $K^{\pm}$ cross section A-dependence in the form of $Ed\sigma_K{}^{\pm}/d^3q \sim A^{\alpha^{\pm}}$. Curve – prediction for K^+ [12]

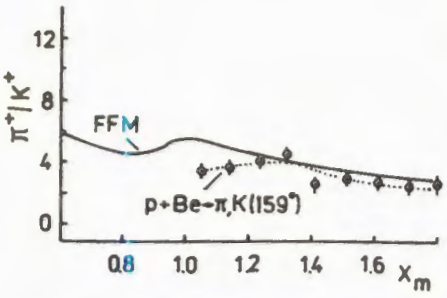

Fig.6. FFM – prediction of the quark model of fluctuon fragmentation [12] for the π^+/K^+-ratio in the reaction $p + d \to \pi^+, K^+(180°)$. Points – our data for Be

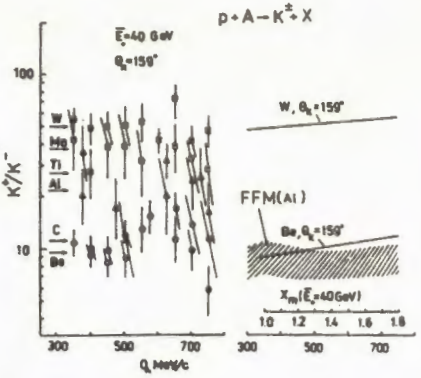

Fig.7. Ratio of the yields of K^+- and K^--mesons. Data for different A are depointed as in figs.1, 2. Arrows are mean values of K^+/K^- for separate A. Linear approximation of $K^+/K^-(x_m)$ and FFM – prediction for the reaction $p + \mathrm{Al} \to K^+(180°) + X$ are shown on the right

quark [12]. The K^+/K^- ratio for our data is shown in fig.7. The observed dependence on x_m corresponds to the assumption of hardness of the quark sea in fluctuons. Figure 7 also shows a quantitative FFM-prediction for the Al nucleus. In this case the observed x_m-dependence does not contradict the predicted one, but the predicted value of K^+/K^- is different. This distinction can be connected with the multiscattering effect as the cross sections of K^+N and K^-N differ substantially at $q_k < 1$ GeV/c.

Conclusion

The momentum and A-dependences of $K^\pm$-production have been measured over a wide range of the cumulative variable $x_m \approx \alpha = 1-1.9$ near 180° (at an angle of 159°, where $q_k^\perp / q_k^\parallel = 0.35$) and in an energy interval of 15—65 GeV, where interactions of projectiles and target constituents take place mainly by far over confinement threshold and therefore quark-parton models of hadron production in nuclear fragmentation can be used as well-grounded ones. The spectra of «sea» hadrons ($K^-, \bar{p}$) make it possible to investigate the difference of the nucleus quark sea from the quark sea of free nucleons. Some predictions of the quark model of fluctuon fragmentation for cumulative kaons (x-dependences) are in accordance with our experimental data. However, correct

taking into account the distortions of the observed hadron spectra due to final state interactions in nuclei is required to compare quantitative model predictions with experimental data.

References

1. Baldin A.M. — Proc. of the 19th Int.Conf. on High Energy Phys., Tokyo, 1978, p.155.
2. Burov V.V., Lukyanov V.K., Titov A.I. — Sov.J.Particles and Nuclei, 1984, vol.15, pp.558—579 (publ. Amer. Inst. Phys.).
3. Efremov A.V. — Prog. Part. Nucl. Phys., 1982, v.8, p.345—365 (Pergamon, New York).
4. Frankfurt L.L., Strikman M.I. — Phys. Rep., 1981, 86, p.215.
5. Baldin A.M. — Sov. J. Particles and Nuclei, 1977, v.8(3), pp.175—195 (publ.Amer. Inst. Phys.).
6. Burov V.V., Lukyanov V.K., Titov A.I. — Phys. Lett., 1977, B67, p.46; JINR Preprint E2-10680, Dubna, 1977.
7. Belyaev I.M. et al. — JINR Communications R1-88-341 and R1-88-342, Dubna, 1988.
8. Gavrishchuk O.P. et al. — Nucl. Phys., 1991, A253, p.589.
9. Boyarinov S.V. et al. — Sov. J. Nucl. Phys., 1989, 50, p.1605.
10. Belyaev I.M. et al. — JINR Communication R1-90-551, Dubna, 1990.
11. Efremov A.V. — Phys. Lett., 1986, B174, p.776.
12. Efremov A.V. et al. — Sov. J. Nucl. Phys., 1988, 47, p.868.

Received on July 16, 1992.

УДК 539.128

80 ps TIMING RESOLUTION SCINTILLATION COUNTER WITH A PHOTOMULTIPLIER TUBE FEU-87

S.V.Afanasiev, Yu.S. Anisimov, A.I.Malakhov, S.G.Reznikov, A.Yu.Semenov, P.I.Zarubin

We describe a TOF scintillator counter with a photomultiplier tube FEU-87 and a 2.4×2.4×6.0 cm^3 scintillator. A time resolution (σ) of 84 ± 4 ps has been obtained from cosmic ray and deuteron beam tests. Possible timing improvements are discussed.

The investigation has been performed at the Laboratory of High Energies, JINR.

Сцинтилляционный счетчик с временным разрешением 80 пс на основе ФЭУ-87

Афанасьев С.В. и др.

Описан времяпролетный сцинтилляционный счетчик на основе фотоумножителя ФЭУ-87 и сцинтиллятора размером 2,4×2,4×6,0 $см^3$. Временное разрешение (σ) 84 ± 4 пс было получено при проведении измерений на космических мюонах и в пучке релятивистских дейтронов. Возможные пути улучшения временных характеристик счетчика обсуждаются.

Работа выполнена в Лаборатории высоких энергий ОИЯИ.

Introduction

The application of the time-of-flight (TOF) method with a typical TOF base of about 12—15 m requires detectors with 50—100 ps timing resolution to provide $\pi-K$ separation up to the momentum of 4—5 GeV/c. In this paper we describe a fast scintillation counter with a Russian photomultiplier tube (PMT) FEU-87 of relatively low cost and a LHE JINR produced scintillator. Our work was initiated by the proposal of the CERN NA-49 collaboration [1]. The described results allow us to improve $\pi-K$ and $K-p$ separation with the SPHERE forward spectrometer [2].

Description of the Counter

We have used a "standard" scintillation material based on polystyrene doped with 1.5% *p*-terphenyl + 0.01% POPOP. The light pulse

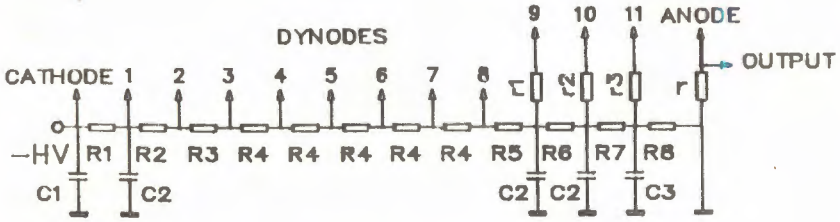

R1 = 560k
R2 = 82k
R3 = 160k
R4 = 100k
R5 = 180k
R6 = 200k
R7 = 220k
R8 = 330k

r1 = 33
r2 = 50
r3 = 100
r = 50

C1 = 4700 pF
C2 = 330 pF
C3 = 33 nF

Fig.1. Voltage divider used with the FEU-87 photomultiplier tube

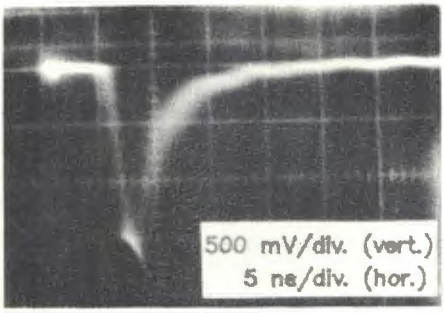

Fig.2. Typical output pulse of the counter

rise time (LPRT) of this scintillator is about 0.8 ns [3]. The scintillator 2.4×2.4×6.0 cm^3 in size was wrapped in black paper without a reflector and viewed from one side (without a light guide) by a fast PMT of the FEU-87 type (2 cm diameter photocathode) with a certificate cathode luminous sensitivity of 95 μA/lm.

A voltage divider (see fig.1) is adjusted to a minimal timing resolution in response to a LED flash. This resolution has been improved by setting a significant voltage (> 700 V) between the protocathode and the first dynode, and thereafter between the last dynodes. No special stabilization is used because a low average working count rate (> 10^5 per second) is expected. The total high voltage is 2800 V. Figure 2 shows an output signal of the counter

(the scintillator is excited with a ^{90}Sr source). An amplitude of about 2 V corresponds to a minimum ionizing particle flash in the counter scintillator.

To estimate the PMT transit time jitter, we have measured the dispersion of time between a LED driving pulse and a PMT output signal for different output pulse amplitudes A (see fig.3). We should note that the observed dispersion behaviour differs significantly from the expected one for the transit time jitter ($\sim A^{-1/2}$ is the dashed line in fig.3). We explain this fact by the existence of a LED time jitter contribution with a more complicated behaviour. Over an amplitude range of about 2 V this contribution is more than 40 ps. On the other hand, in our measurements the photocathode is illuminated by a LED flash not quite uniformly. This fact means the existence of an additional unmeasured contribution to the PMT transit time dispersion (though its value should be not very significant because of the high voltage between the cathode and the first dynode). Finally, we estimate the PMT transit time jitter as about 50—60 ps.

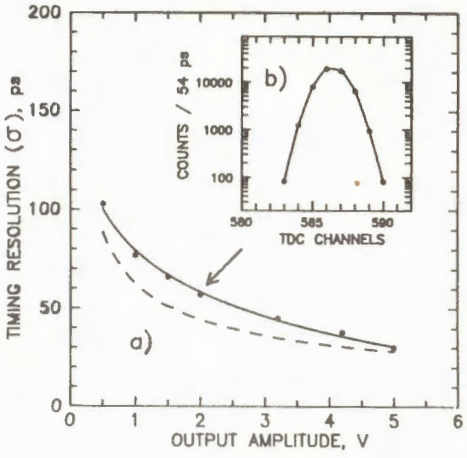

Fig.3. a) Dispersion of time between a LED driving pulse and a PMT output amplitude. The dashed line corresponds to the $A^{-1/2}$ dependence. b) Time spectrum for an amplitude of 2 V

Cosmic Ray Tests

A preliminary measurement of counter timing resolution was carried out with cosmic rays. A schematic drawing of the test arrangement is shown in fig.4. It includes:

— a test counter S;

— a cosmic muon telescope consisting of two 2.0 cm thick $1.0 \times 1.0\ cm^2$ scintillators viewed by FEU-87 PMTs;

— constant fraction discriminators produced at LHE;

— a CAMAC readout system including TDCs (54 ps/channel), an ADC and a crate-controller with an IBM PC/XT compatible computer.

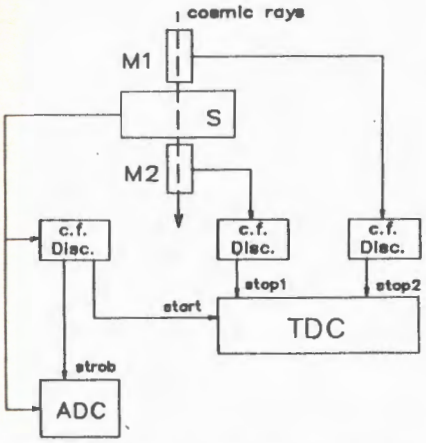

Fig.4. Schematic drawing of the cosmic ray test arrangement

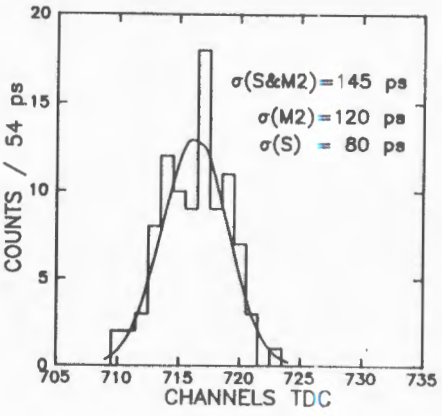

Fig.5. TOF spectrum for cosmic muons

Cosmic rays monitor rate was about 10 counts per hour and it took about 8 hours for one exposure.

Timing was done between S and $M1$, S and $M2$. Stop signals for TDCs were provided by both counters of the muon telescope and common start by the test counter S. The pulse charge of the counter S was also measured. A cut was set on this pulse charge in order to select minimum ionizing particles in cosmic radiation. The obtained S — $M2$ time spectrum corrected for residual amplitude dependence is presented in fig.5. The timing resolution σ_S of the counter S is obtained from $\sigma_{S\&M1}$, $\sigma_{S\&M2}$ and $\sigma_{M1\&M2}$. The last value is obtained from event-by-event subtraction $\mathrm{TOF}_{S\&M1} - \mathrm{TOF}_{S\&M2}$. The test counter time resolution derived from the corrected spectra is $\sigma_S \approx 80$ ps.

Deuteron Beam Tests

As a continuation of our study, we carried out tests on a 9 GeV/c deuteron beam. A layout of the test assembly is shown in fig.6. It includes:

— a test counter S;

— two monitor counters; the thickness of the forward one is 2.0 cm and its entrance area 1.0×1.0 cm^2; the thickness and diameter of the rear one is 10 cm and 1 cm, respectively; PMTs are FEU-87.

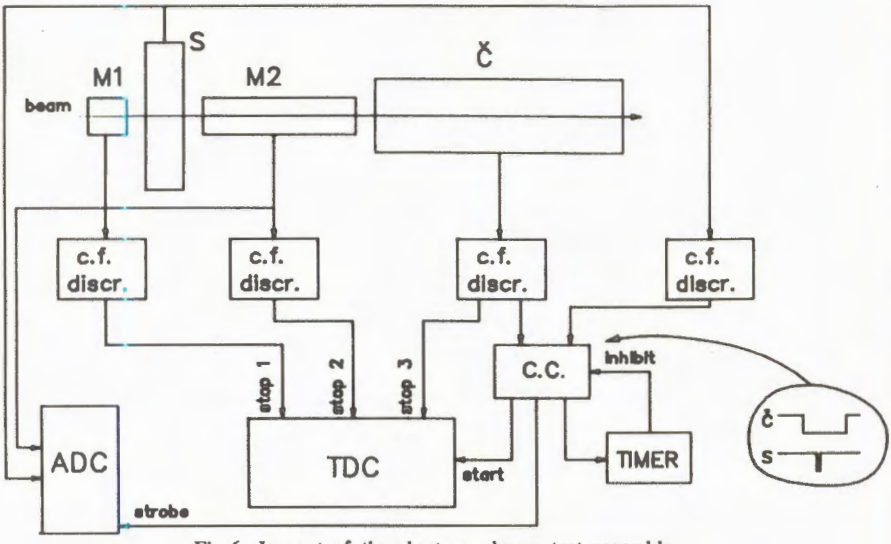

Fig.6. Layout of the deuteron beam test assembly

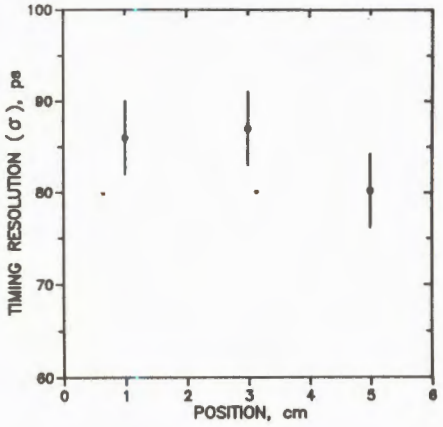

Fig.7. Position dependence of the counter S timing resolution

— an additional Cherenkov plexiglass counter C 20 cm thick and 2.5 cm in diameter; its radiator is viewed by a FEU-85 type PMT (it has a higher gain than FEU-87);

— fast logic modules and a CAMAC readout system.

Data were read out in coincidence between the counters S and C. The output signal of the coincidence unit was timed with the pulse of the counter S pulse. Timing was done between S and $M1$, S and $M2$, S and C as well as charge measurements of $M2$ and S signals. A timer gate decreases a trigger rate down to 200—300 per spill. Deuterons having passed through the whole assembly are selected by applying cuts on TOF ($S-C$) and ADC ($M2$). The timing resolution σ_S of the counter S is obtained as shown above. The position dependence of σ_S is shown in fig.7 for a PMT with a cathode

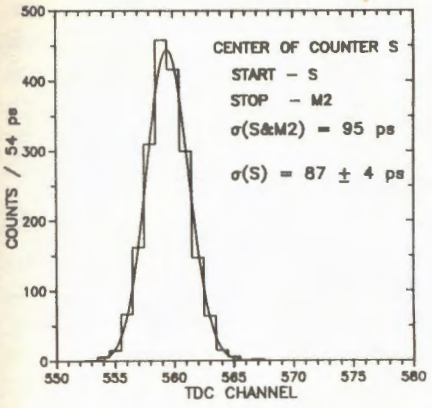

Fig.8. TOF spectrum for 9GeV/c deuterons

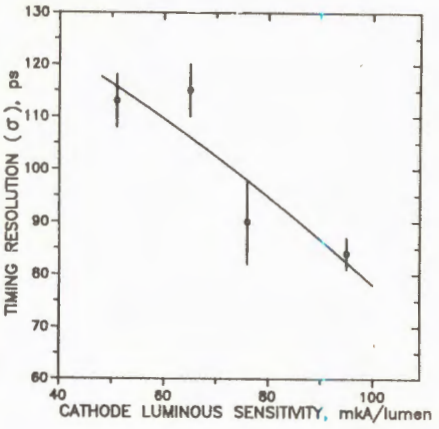

Fig.9. Counter S timing resolution vs the cathode luminous sensitivity of PMT

luminous sensitivity of 95 μA/lm. The mean value of $\langle\sigma_S\rangle$ is equal to 84 ± 1.5 (stat.) ± 4 (sys) ps. The systematic error is associated with PMT timing instability. The TOF ($S-M2$) spectrum obtained at the center of the counter S is shown in fig.8.

Besides, the σ_S dependence on the cathode luminous sensitivity of PMT (see fig.9) was estimated. The value of sensitivity was taken from the PMT certificate. The 85 μA/lm lower limit can be put as a selection criterion of PMTs acceptability.

We note that the beam tests confirmed the conclusions derived from the cosmic ray run.

Some Possible Improvements

Here we would like to discuss possible ways to improve timing parameters of the counter.

One way to improve timing parameters of the scintillation counter is to use scintillation material with the shorter LPRT. For example, a scintillator based on polystyrene doped with 1.5—2.0% p-terphenyl (without any secondary dyes) has the LPRT of about 75 ps [3]. However the light yield obtained from this scintillator is only about 60% of that of our "standard" scintillator and additional tests to study this problem are needed.

A possible improvement of PMT's timing parameters is due to employing an inverse pulse from a dynode as an outpot one. First, this operation provides smaller inner PMT's stray capacitance and a decrease of electron pulse widening [4] and, second, it eliminates the anode signal parasitic component induced by electrons travelling from the penultimate dynode to the last dynode [5]. In this way we hope to decrease significantly the PMT time jitter.

The authors express their sincere gratitude to the members of the Dubna Synchrophasotron staff and the beam transport group for the high quality deuteron beam. Also the authors are much indebted to Dr.A.I.Golokhvastov for his continuous interest and valuable discussion.

References

1. Large Acceptance Hadron Detector for an Investigation of Pb-Induced Reactions at CERN SPS. NA-49 Collaboration, CERN SPSLC 91-31 SPSLC/P264.
2. Anisimov Yu.S. et al. - JINR Rapid Communications, N5-91, Dubna, 1991, p.23.
3. Matveeva E.N. et al. - Nucl. Instr. and Meth. 1981, 179, p.277.
4. Beck G. - Rev. Sci. Instrum. 1976, 47, No.5, p.537.
5. Bengtson B. , Moszynski M. - Nucl. Instr. and Meth., 1982, 204, p.129.

Received on June 19, 1992.

УДК 539.122:539. 12...162.6/8

RADIAL PROFILES OF PHOTON INITIATED ELECTROMAGNETIC SHOWERS BETWEEN 100 AND 3500 MeV

B.Słowiński, J.Rogulski

It is shown that the radial dependence of the density of shower electrons ionization loss may be approximated by some universal function $F(x)$ of the dimensionless variable x only. This function has its asymptotics as $F(x) \sim e^{-x}$ at large enough x.

The investigation has been performed at the Laboratory of High Energies JINR (Dubna) and at the Institute of Physics, Warsaw University of Technology (Warsaw).

Радиальные профили электромагнитных ливней, вызываемых гамма-квантами с энергией 100—3500 МэВ

Б.Словинский, Я.Рогульский

Показано, что радиальная зависимость плотности ионизационных потерь ливневых электронов может быть аппроксимирована некоторой универсальной функцией $F(x)$, зависящей только от безразмерной переменной x. При достаточно больших x асимптотикой этой функции является экспонента: $F(x) \sim e^{-x}$.

Работа выполнена в Лаборатории высоких энергий ОИЯИ (Дубна) и в Институте физики Варшавского технического университета (Варшава).

I. Introduction

It has been found earlier[1] that the average radial profile $E_r(r|E_\gamma, t)$ of showers created in liquid xenon by gamma quanta of energy E_γ = 100—3500 MeV is related with the corresponding plane distribution $f_p(p|E_\gamma, t)$ of shower electrons ionization loss according to the equation:

$$f_p(p|E_\gamma, t) = 2\int_p^\infty \frac{F_r(r|E_\gamma, t)}{\sqrt{1-(p/r)^2}}\, dr, \qquad (1)$$

where r is a distance from the shower axis (SA), p is its projection in the picture plane, in which the normalized density of partial summary projection ranges $f_p(p|E_\gamma, t)$ of shower electrons was measured within

squares having sides $\Delta t = 0.6$ radiation length (rl) along the SA and $\Delta p = 0.3$ rl. As a result of the fit to the experimental data of exponential function

$$f_p(p|E_\gamma, t) = \frac{1}{\bar{p}(E_\gamma, t)} e^{-p/\bar{p}(E_\gamma, t)} \tag{2}$$

the following parametrization of the average plane shower width was obtained[2]:

$$\bar{p}(E_\gamma, t) = \alpha + \beta(E_\gamma) \cdot t. \tag{3}$$

Here $\alpha = (4.2 \pm 1.2) \cdot 10^{-2}$ rl, $\beta(E_\gamma) = a - b \cdot \ln E_\gamma$, $a = (7.5 \pm 0.3) \cdot 10^{-2}$, $b = (6.6 \pm 0.4) \cdot 10^{-3}$ when E_γ is in MeV.

The equation has a unique solution of the form[1]:

$$F_r(r|E_\gamma, t) = \frac{1}{\pi r^2} \int_\infty^r \frac{d}{dp} [p \cdot f_p(p|E_\gamma, t)] \frac{dp}{\sqrt{1 - (r/p^2)}} . \tag{4}$$

Substituting the function (2) into (4) we can obtain the exact formula for the average radial distribution of ionization loss in electromagnetic showers.

In the present work we show that this distribution may be expressed by means of a universal function determining its radial shape.

II. Radial Shower Profile

Let us denote for short: $\bar{p} = \bar{p}(E_\gamma, t)$, $x = r/\bar{p}$, $s = r/p$ and $F_r(x) = F_r(r|E_\gamma, t)$. Then from (4) and (2) we have

$$F_r(x) = \frac{1}{\pi \bar{p}^2} \cdot F(x) , \tag{5}$$

where the function

$$F(x) = \int_0^1 \frac{\frac{1}{s} - \frac{1}{x}}{s^2 \sqrt{1 - s^2}} e^{-x/s} ds , \tag{6}$$

depending on the dimensionless variable x, determines the radial behaviour of the density $F_r(x)$ of shower electrons ionization loss, whereas all information about the primary photon energy E_γ as well as

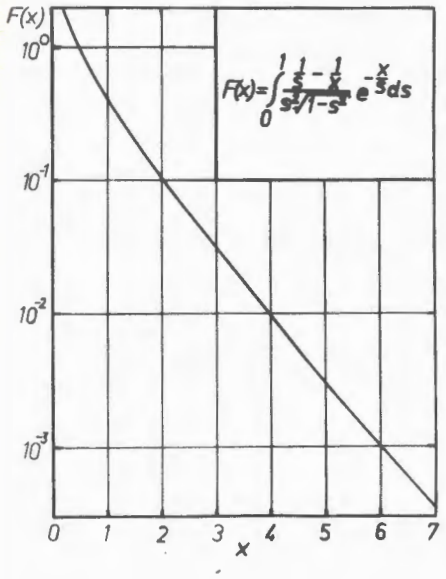

Radial dependence of the density of shower electrons ionization lass

(homogeneous) absorbent properties and a shower depth t is contained in the parameter $\bar{p}$. The figure displays the function (6) within the interval of $x = 0.2—7$.

It is to be shown strictly that at higher values of x $(x \geq 2)$ $F(x) \sim e^{-x}$ as can be seen in the figure.

Mention finally the suggestion/3/ that the solution of (1) is as follows

$$F_r(r) = \frac{1}{\pi \bar{p}^2} K_0(x) , \qquad (7)$$

where $K_0(x)$ is the McDonald function. But then it would satisfy the equation:

$$r^2 F_r''(r) + r F_r'(r) - (\frac{r}{\bar{p}})^2 F_r(r) = 0 \qquad (8)$$

which is not the case.

References

1. Słowiński B. — Proc. of the Intern. Meeting on Problems of Mathemat. Simulation in Nuclear Physics Researches, 30 Sept.—2 Oct., 1980. JINR D10,11-81-622, Dubna, 1981, p.178.
2. Słowiński B. — JINR E1-89-789, Dubna, 1989.
3. Kostritsa A.A. — Report of IPHE 87-20, Alma-Ata, 1988.

Received on February 5, 1992.

УДК 539.12.172

ФОРМФАКТОРЫ НУКЛОНА И КВАРКОВ В МОДЕЛИ РЕЛЯТИВИСТСКОГО ГАРМОНИЧЕСКОГО ОСЦИЛЛЯТОРА С УЧЕТОМ СПИНА КВАРКОВ

В.В.Буров, С.М.Доркин[1], А.Де Паче[2], П.Саракко[3]

Показано, что в рамках модели релятивистского гармонического осциллятора с учетом спина кварков и условия скейлинга можно описать зарядовый, магнитный и аксиальный формфакторы нуклона. Получено, что среднеквадратичный радиус нуклона равен 0,74 фм и размер кварка 0,36 фм.

Работа выполнена в Лаборатории теоретической физики ОИЯИ.

Nucleon and Quark Form Factors in Relativistic Harmonic Oscillator Model

V.V.Burov, S.M.Dorkin, A.De Pace, P.Saracco

It is shown that the nucleon charge, magnetic and axial factors can be explained in the framework of relativistic harmonic oscillator model with taking into account a spin of quarks and the scaling rule. It is found that the nucleon rms radius is equal to 0.74 fm and the quark size is 0.36 fm.

The investigation has been performed at the Laboratory of Theoretical Physics, JINR.

В данной работе рассмотрим электромагнитные и слабый формфакторы нуклона в рамках модели релятивистского гармонического осциллятора (МРГО). Исследования в рамках этой модели проводились в работах [1—13]. Здесь следует выделить работы [7—11], посвященные формфакторам нуклонов. В этих работах исследовались зарядовый $G_E^{p,n}(q^2)$, магнитный $G_M^{p,n}(q^2)$ формфакторы нуклонов, и, кроме того, в работе [9] изучался аксиальный формфактор нуклона $G_A(q^2)$. Важной особенностью МРГО является дипольного типа асимптотическое поведе-

[1]Дальневосточный государственный университет, Владивосток, Россия
[2]Национальный институт ядерной физики, Турин, Италия
[3]Национальный институт ядерной физики, Генуя, Италия

ние магнитного формфактора нуклона при $q^2 \to \infty$, что соответствует правилам кваркового счета [14,15]. Такая q^2-зависимость появляется из-за интеграла перекрытия волновых функций внутреннего движения кварков в поле релятивистского осциллятора, объясняя лоренцевское сокращение как следствие решения уравнения МРГО с граничным условием [3] (см. также [4]). Здесь следует отметить, что для того, чтобы объяснить электромагнитные и аксиальный формфакторы нуклона, необходимо построить спин-унитарную спинорную часть волновой функции и вершинную функцию системы со спином 1/2. В работе [5] был дан метод вычисления ковариантного и калибровочно-инвариантного тока в рамках $\bar{U}(12) \otimes O(3,1)$-модели. Однако имелись определенные проблемы в этом подходе (см., например, лекции [16]). В работах [7—9] были получены ковариантный и калибровочно-инвариантный ток в случае $SU(6) \otimes O(3,1)$-модели и было показано, что можно добиться удовлетворительного описания магнитного, зарядового и аксиального формфакторов нуклона. Однако согласие с экспериментальными данными при этом значительно хуже, чем, например, в нерелятивистской модели, учитывающей лоренцевское сжатие волновой функции нуклона [17].

Целью настоящей работы является описание формфакторов нуклона в модели релятивистского гармонического осциллятора с использованием $SU(6) \otimes O(3,1)$-схемы получения ковариантного и калибровочно-инвариантного тока на основе предположения о том, что поведение формфакторов при $q^2 \to \infty$ определяется правилами кваркового счета [14,15] и что выполняется экспериментально наблюдаемый скейлинг формфакторов нуклонов $G_E^p(q^2) = \dfrac{G_M^p(q^2)}{\mu_p} = \dfrac{G_M^n(q^2)}{\mu_n}$, где $\mu_{n,p}$ — магнитные моменты нейтрона и протона.

Рассмотрим систему, состоящую из N кварков, в поле релятивистского гармонического осциллятора. Тогда волновую функцию можно представить в виде:

$$\Psi_P^{(N)}(x_1,\ldots,x_N) = \hat{A}\Phi_N(x_1,x_2,\ldots x_N)U^{(N)}(\mathbf{P}). \qquad (1)$$

Здесь $\hat{A}$ — оператор антисимметризации кварков, включая цветовые степени свободы, которые для простоты явно выписывать не будем, $\Phi_N(x_1,x_2,\ldots x_N)$ — ковариантная пространственно-временная волновая функция и $U^{(N)}(\mathbf{P})$ — спиновая волновая функция (их коротко опишем ниже). Пусть волновая функция Φ_N удовлетворяет уравне-

нию Клейна — Гордона с релятивистским гармоническим осцилляторным потенциалом [1—13]

$$\left\{\sum_{i=1}^{N} p_i^2 + K^2\left[\sum_{i>j}^{N}\sum_{j=1}^{N-1}(x_i - x_j)^2\right]\right\}\Phi_N(x_1, x_2, \ldots x_N) = 0, \tag{2}$$

где $p_i = -i\partial/\partial_{x_i}$ — 4-импульс, K — осцилляторный параметр, x_i — 4-координата i-го кварка (имея в виду изоспиновую симметрию, будем считать массы кварков одинаковыми). Тогда, переходя к координатам центра масс X и внутренним переменным $r_0, \ldots r_{N-1}$, представим уравнение (2) в виде:

$$(P^2 - M_p^2)\Phi_{Nq}(r_0, r_1, \ldots r_{N-1}, P) = 0, \tag{3}$$
$$M_p^2 = -2\alpha_N a_{i\mu}^{+} a_{i\mu} = 0, \quad \alpha_N = KN\sqrt{N},$$

где $a_{i\mu}$, $a_{i\mu}^{+}$ — операторы рождения и уничтожения частиц. Решение данного уравнения (с учетом условия Такабаяши [3], необходимого для устранения нефизических колебаний по координате относительного времени $P^\mu a_{i\mu}^{+}\Phi_{Nq} = 0$) будет иметь следующий вид:

$$\Phi_N\left(r_0, r_1, \ldots r_{N-1}, P\right) = \left(\frac{\alpha_N}{\pi N}\right)^{N-1} \exp\left(\frac{\alpha_N}{2N} K^{\mu\nu} \sum_{i=1}^{N-1} r_{i\mu} r_{i\nu}\right), \tag{4}$$

$$\Phi_N\left(x_1, x_2, \ldots x_N\right) = \exp\left[iP_\mu X_\mu\right]\Phi_N\left(r_0, r_1, \ldots r_{N-1}, P\right), \tag{5}$$

где P — полный импульс системы и $K^{\mu\nu} = g^{\mu\nu} - 2P^\mu P^\nu / P^2$. Спиновую волновую функцию в движущейся системе можно построить (см. работы [8—12]), преобразовав нерелятивистскую спиновую волновую функцию в лабораторной системе. Это можно проделать двумя способами. Первый способ — преобразовать волновую функцию каждого кварка отдельно как дираковский спинор, используя уравнение Баргманна — Вигнера. Второй — преобразовать волновую функцию всей системы как целое (так называемое минимальное преобразование Паули), т.к. при этом волновая функция имеет минимальное число компонент. Второй путь, по-видимому, предпочтительнее, т.к. в отличие от первого способа позволяет получить зарядовый формфактор нейтрона не равным тождественно нулю. Далее мы будем рассматривать второй способ, следуя работе [12]. Тогда спиновая волновая функция $U^{(N)}(\mathbf{P})$ может быть представлена в виде:

$$U^{(N)}(\mathbf{P}) = B(\mathbf{P})U^{(N)}(0),$$

$$B(\mathbf{P}) - \exp\left[\frac{b}{2|P|}\rho_1(\mathbf{P}\cdot\vec{\sigma})\right] = \exp\left[\rho_1 bH\right], \tag{6}$$

где $H = (\mathbf{P}\vec{\sigma})/2|\mathbf{P}|$, $b = \cosh^{-1}P_0/M$, и $\vec{\sigma} \equiv \sum_{i=1}^{N} \vec{\sigma}, \vec{\sigma}$ — матрицы Паули i-го кварка и $U^{(N)}(0)$ — волновая функция в лабораторной системе:

$$U^{(N)}(0) = \begin{pmatrix}\chi\\0\end{pmatrix} \tag{7}$$

(здесь χ — нерелятивистская спиновая функция системы) . Следуя работам [6,9,12], запишем электромагнитный ток в виде:

$$I_{em} = \int \prod_{i=1}^{N} dx_i \sum_{k}^{N} j_{k\mu}(x_1,\ldots,x_N)\, A_\mu(x_k), \tag{8}$$

где

$$j_{k\mu}(x_1,\ldots,x_N) = -i\overline{\Psi}^{(N)} N e_k \times \tag{9}$$

$$\times \left[g_E(q^2)\frac{\overleftrightarrow{\partial}}{\partial x_{k\mu}} + ig_M(q^2)\,\sigma^k_{\mu\nu}\left(\frac{\vec{\partial}}{\partial_{k\nu}} + \frac{\overleftarrow{\partial}}{\partial x_{k\nu}}\right)\right]\Psi^{(N)}.$$

Здесь $\Psi^{(N)}, \overline{\Psi}^{(N)}$ — начальная и конечная волновые функции N-кварковой системы (2), e_k — заряд k-го кварка, $\sigma^k_{\mu\nu}$ — спиновые матрицы k-го кварка ($\sigma^k_{ij} \equiv \varepsilon_{ijl}\sigma^k_l$, $\sigma^k_{i4} = \sigma^k_{4i} \equiv \rho_1\sigma^k_i$). В предположении неточечности кварков определим $g_E(q^2)$ и $g_M(q^2)$ как зарядовый и магнитный формфакторы кварков ($q = p' - p$ — переданный 4-импульс для N-кварковой системы с начальным (конечным) 4-импульсом $p_\mu(p'_\mu)$). Подставляя волновую функцию (5) в уравнения для тока (8), (9) и вычисляя интегралы по переменным кварков $x_1,\ldots,x_N$, получаем эффективный ток для N-кварковой системы с $p_\mu(p'_\mu)$ и спиновой компонентой $s(s')$:

$$\langle p's'|J^{(N)}_\mu(0)|ps\rangle = \frac{I^{(N)}(q^2)}{\sqrt{2p_0p'_0}}\sum_{k=1}^{N}(\overline{U}^{(N)}_{s'}(\mathbf{p}')\,\Gamma_{k\mu}\,U^{(N)}_s(\mathbf{p})), \tag{10}$$

где

$$\Gamma_{k\mu} = \left[(p_\mu + p'_\mu)\,I_N(q^2)\,g_E(q^2) - iNg_M(q^2)\sigma^k_{\mu\nu}q_\nu\right]. \tag{11}$$

$$\Gamma_{k\mu} = \left[(p_\mu + p'_\mu)\, I_N(q^2)\, g_E(q^2) - iNg_M(q^2)\sigma^k_{\mu\nu}q_\nu\right]. \qquad (11)$$

Здесь интегралы по пространственно-временным переменным имеют следующий вид:

$$I^{(N)}(q^2) = \frac{1}{(1 + q^2/2M^2)^{(N-1)}} \exp\left[-\frac{N-1}{4\alpha_N}\left(\frac{q^2}{1 + q^2/2M^2}\right)\right], \qquad (12)$$

$$I_N(q^2) = \frac{1 + Nq^2/2M^2}{1 + q^2/2M^2}, \qquad (13)$$

где M — масса системы. Используя (6) и волновую функцию в лабораторной системе (7), преобразуем (10) для трехкварковой системы и получим окончательные выражения для формфакторов нуклона. Так, для магнитного формфактора протона и нейтрона имеем:

$$F^p_M(q^2) = \frac{G^p_M(q^2)}{\mu_p} = \frac{G^n_M(q^2)}{\mu_n} = g_M(q^2)I^{(3)}(q^2), \qquad (14)$$

для электрического формфактора протона получаем выражение

$$F^p_E(q^2) = G^p_E(q^2) = \left[\left(1 + \frac{q^2}{2M^2}\right) I_3(q^2)\, g_E(q^2) - \frac{3q^2}{4M^2} g_M(q^2)\right] I^{(3)}(q^2) \qquad (15)$$

и, наконец, для электрического формфактора нейтрона:

$$F^n_E(q^2) = \frac{q^2}{2M^2} g_M(q^2)I^{(3)}(q^2). \qquad (16)$$

Можно также вычислить аксиальный формфактор нуклона $F_A(q^2) = G_A(q^2)/G_A(0)$ (определение и детали вычислений можно найти в работе [9]):

$$F_A(q^2) = G_A(q^2)/G_A(0) = g_E(q^2)I_3(q^2)I^{(3)}(q^2). \qquad (17)$$

Отметим, что в $SU(6)$-модели магнитный момент протона $\mu_p = 3$, а нейтрона $\mu_n = -2$, что отличается от соответствующих экспериментальных значений $\mu_p = 2{,}7928474$ и $\mu_n = -1{,}91304275$. Поэтому при дальнейшем анализе экспериментальных формфакторов нуклона последние будем нормировать на 1 при $q^2 = 0$. В выражениях (13) и (14—17) $M = 0{,}93828$ ГэВ — масса нуклона.

Далее проанализируем выражения для магнитного и зарядового формфакторов нуклона. Из условия скейлинга следует, что $F_M^p(q^2) = F_E^p(q^2)$. Отсюда легко получить выражение для *зарядового формфактора кварка* $g_E(q^2)$:

$$g_E(q^2) = \frac{(1 + 3q^2/4M^2)(1 + q^2/2M^2)}{(1 + q^2/4M^2)(1 + 3q^2/2M^2)} g_M(E). \qquad (18)$$

Согласно правилам кваркового счета [14,15] формфактор нуклона при $q^2 \to \infty$ убывает как q^{-4}. При $q^2 \to \infty$ $F_M^p(q^2) \sim g_M(q^2)/q^4$, поэтому естественно предположить, что $g_M(q^2) = 1$, оставляя при этом возможность модифицировать асимптотическое поведение формфакторов за счет введения дополнительного, например, логарифмического убывания $g_M(q^2)$ при $q^2 \to \infty$.

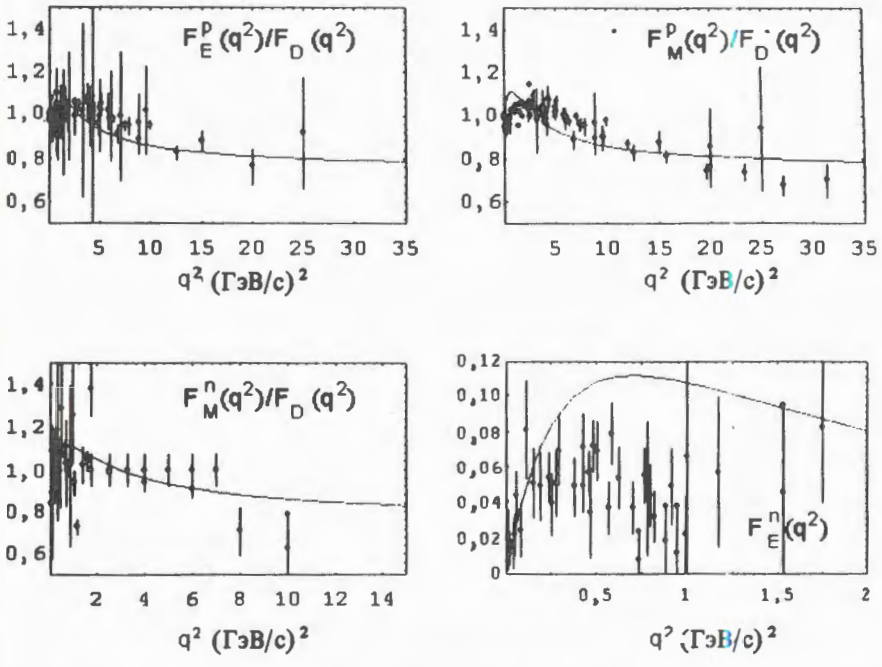

Рис.1. Отношение нормированных формфакторов нуклона $F_{E,M}^{p,n}(q^2)$ к дипольному формфактору (19). Экспериментальные данные взяты из работ [19—34]

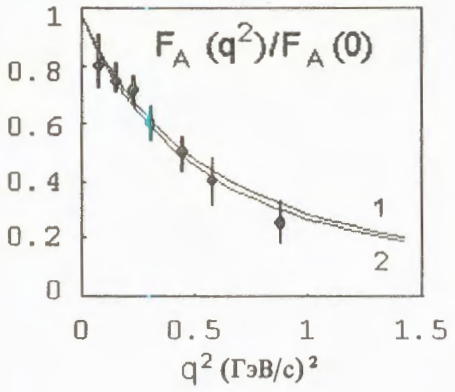

Рис.2. Нормированный аксиальный формфактор нуклона $F_A(q^2) = G_A(q^2)/G_A(0)$. Кривая 1: расчет по модели МРГО (17), 2 – дипольный фит (19) [37]. Точки — BNR-анализ из работы [38].

Осцилляторный параметр определим из фитирования (14) к экспериментальным данным для магнитного и зарядового формфакторов протона. Этот параметр оказался равным $\alpha_3 = 0{,}42$ ГэВ/с^2, что согласуется с результатами работы [9].

Далее вычислим по формуле (15) теоретическое значение наклона электрического формфактора при $q^2 = 0$: $dF_E^n(q^2)/dq^2|_{q^2=0} = 0{,}022$, что соответствует известному экспериментальному значению $0{,}0202 \pm 0{,}0003$ фм^2 [18]. На рис.1 и 2 показано сравнение с экспериментальными данными [19—34] (см. также работы [35] и [36]) отношения формфакторов нуклона в модели МРГО к известному дипольному формфактору:

$$E_D(q^2) = \frac{1}{(1 + q^2/\Lambda^2_{E,A})^2}, \qquad (19)$$

где для электромагнитных формфакторов $\Lambda^2_E = 0{,}71$ (ГэВ/с)^2 и для аксиального $\Lambda^2_A = 1{,}02$ (ГэВ/с)^2 [37].

Напомним, что зарядовый и магнитный формфакторы подгонялись к экспериментальным данным (первые два графика на рис.1), а остальные получены без дополнительных параметров. Видно хорошее согласие с магнитным и зарядовым формфакторами нейтрона.

Также наблюдается хорошее согласие аксиального формфактора нуклона (17) с экспериментом [37,38] (рис.2). Причем последний прямо зависит от зарядового формфактора кварка (18).

Используя уравнения (15), (14) и (18), оценим размеры нуклона $\bar{r}_{(p,n)} = \sqrt{\langle r^2_{(p,n)}\rangle} = \sqrt{6(1/2\alpha_3 + 1/M^2)}$ и кварка $\bar{r}_q = \sqrt{\langle r^2_q\rangle} = \sqrt{3/M^2}$. Отсюда получаем, что $\bar{r}_{(p,n)} = 0{,}74$ фм, что согласуется с экспериментальными данными, и $\bar{r}_q = 0{,}36$ фм.

Представленная модель позволяет довольно просто объяснить совокупность экспериментальных данных по формфакторам нуклона при использовании всего одного подгоночного параметра. Этот факт позволяет надеяться на то, что в данной модели хорошо описывается структура нуклона. При этом приходится использовать предложение о неточечности кварков, которое может быть в дальнейшем проверено в других процессах (например, можно вычислить сильную πNN-вершину, формфакторы Δ-изобары, структурные функции и др.). Кроме того, данная модель легко обобщается на случай систем с числом кварков больше трех.

Литература

1. Yukawa H. — Phys. Rev., 1953, v.91, p.416.
2. Марков М.А. — Гипероны и К-мезоны. М.: Физматгиз, 1958.
3. Takabayashi T. — Phys. Rev.B, 1965, 139, B1381; Suppl. Prog. Theor. Phys., 1979, 67, p.1.
4. Fujimura K., Kobayashi T., Namiki M. — Prog. Theor. Phys., 1971, 51, p.1152.
5. Feynman R.P., Kisslinger M., Ravndal F. — Phys. Rev. D, 1971, 3, p.2706.
6. Lipes R.G. — Phys. Rev. D, 1972, 5, p.2849.
7. Blagojevic M., Lalovic D. — Prog. Theor. Phys., 1974, 51, p.1152.
8. Ishida S., Matsuda A., Namiki M. — Prog. Theor. Phys., 1977, 57, p.210.
9. Saito S. — Prog. Theor. Phys., 1977, 58, p.1802.
10. Kizukuri Y. et al. — Prog. Theor. Phys., 1979, 61, p.559.
11. Kizukuri Y. et al. — Prog. Theor. Phys., 1980, 64, p.1478.
12. Honzawa N. et al. — Prog. Theor. Phys., 1985, 73, p.1502.
13. Burov V.V. et al. — In: Relativistic Nuclear Physics & Quantum Chromodynamics, ed. by Baldin A.M., Burov V.V., Kaptari L.P., World Scientific, 1990, p.266.
14. Matveev V.A., Muradyan R.M., Tavkhelidze A.N. — Lett. Nuovo Cim., 1973, 7, p.719.
15. Brodsky S., Farrar G. — Phys. Rev. Lett., 1973, 31, p.1153.
16. Feynman R.P. — In: Photon-Hadron Interactions, W.A.Benjamin, Inc., Reading, Massachusetts, 1972.
17. Beyer M., Singh S.K. — Phys. Lett., 1985, 160B, p.26.
18. Koester L. et al. — Phys. Rev. Lett., 1976, 36, p.1021.
19. Rock S. et al. — Phys. Rev. Lett., 1982, 49, p.1139.
20. Bartel W. et al. — Phys. Lett., 1972, 39B, p.407.
21. Budnitz R.J. et al. — Phys. Rev., 1968, 173, p.1357.

22. Stein P. et al. — Phys. Rev. Lett., 1966, 16, p.592.
23. Danning J.R. et al. — Phys. Rev., 1966, 141, p.1286.
24. Hughes E.B. et al. — Phys. Rev. B, 1965, 139, p.458.
25. Akerlof C.W. et al. — Phys. Rev. B, 1964, 135, p.810.
26. Albrecht W. et al. — Phys. Lett., 1968, 26B, p.642.
27. Berger Ch. et al. — Phys. Lett., 1971, 35B, p.87.
28. Bartel W. et al. — Phys. Lett.B, 1970, 33B, p.245.
29. Bartel W. et al. — Nucl. Phys. B, 1973, B58, p.429.
30. Albrecht W. et al. — Phys. Rev. Lett., 1966, 17, p.1192.
31. Janssens T. et al. — Phys. Rev., 1965, 142, p.922.
32. Kirk P.N. et al. — Phys. Rev. D, 1973, 8, p.63.
33. Hansen K. et al. — Phys. Rev. D, 1973, 8, p.753.
34. Bosted P. et al. — In: Relativistic Nuclear Physics & Quantum Chromodynamics, ed. by Baldin A.M., Burov V.V., Kaptari L.P., World Scientific, World Scientific, 1990, p.276.
35. Gari M., Krümpelmann W. — Phys. Lett. B, 1984, 141, p.295.
36. Blatnik S., Zovko N. — Acta Physica Austriaca, 1974, 39, p.62.
37. Miller K.L. et al. — Phys. Rev. D, 1982, 26, p.537.
38. Amaldi E. et al. — Springer Tracts in Modern Physics, v.83, Berlin, 1979.

Рукопись поступила 15 июня 1992 года.

УДК 539.125.523.348+539.126.4

SUBTHRESHOLD ρ AND J/ψ PRODUCTION ON NUCLEI (MONTE — CARLO SIMULATION)

M.Penţia[1], D.Pop[1], N.Ghiordănescu[2], A.G.Litvinenko, A.I.Malakhov, G.L.Melkumov, P.I.Zarubin, V.K.Bondarev[3]

The vector meson production, below the nucleon-nucleon kinematical limit, was studied by extending the general cross section description for stable particle subthreshold production. The final state particle distributions due to ρ and J/ψ meson production and subsequent decay were investigated by Monte — Carlo simulation and phase space integration.

The investigation has been performed at the Laboratory of High Energies, JINR.

Подпороговое образование резонансов ρ и J/ψ на ядрах (Моделирование методом Монте — Карло)

М.Пенция и др.

Проанализирован процесс рождения векторных мезонов за кинематическим пределом нуклон-нуклонных соударений с помощью обобщения сечения рождения стабильных кумулятивных частиц. Распределения частиц от распада резонансов ρ и J/ψ исследовались методом Монте — Карло и интегрированием по фазовому пространству.

Работа выполнена в Лаборатории высоких энергий ОИЯИ.

1. Subthreshold Particle Production

A lot of experimental and theoretical works [1—6] on high momentum transfer relativistic nuclear reactions are studying the particle production below the kinematical limit of the nucleon-nucleon interaction. Generally, in an inclusive nucleus-nucleus interaction:

$$A + B \to 0 + ... + X \qquad (1)$$

the threshold for the 0 denoted particle production can be related to the x_A and x_B scale variable [4]. It represents the fraction of the p_A and p_B 4-momentum of the target and beam particle that could produce

[1]Institute for Nuclear Physics and Engineering, Bucharest, Romania
[2]Bucharest University, Romania
[3]St. Petersburg University, Russia

the 0 particle with a given p_0, for the minimum of the squared total CM energy of the interacting constituents:

$$s = (x_A \cdot p_A + x_B \cdot p_B)^2. \tag{2}$$

It means the experimental particle spectra can be described [6] by the minimum value s_{min}. It is expressed by the 4-momentum conservation law and condition of minimum:

$$\begin{cases} (x_A \cdot p_A + x_B \cdot P_B - p_0)^2 = M_X^2 \\ \dfrac{ds}{dx} = 0, \end{cases} \tag{3}$$

which give the x_A and x_B values along with the s_{min} one.

If x_A and x_B are expressed in nucleon mass fraction:

$$X_A = \frac{x_A \cdot m_A}{m_N}, \quad X_B = \frac{x_B \cdot m_B}{m_N}, \tag{4}$$

the new variables, when they are $X_A > 1$ or $X_B > 1$, formally define the subthreshold production processes.

The differential cross section for the general process (1) is expressed by the square of the matrix element $|\mathcal{M}|^2$, by the primary particles flux density Φ and the Lorentz invariant phase space element dLips [7]:

$$d\sigma = \frac{|\mathcal{M}|^2}{\Phi} \text{dLips} =$$

$$= \frac{|\mathcal{M}|^2}{4\sqrt{(p_A p_B)^2 - m_A^2 m_B^2}} (2\varphi)^2 \sigma^4 \left[p_A + p_B - (p_0 + \ldots + p_X)\right] \times \tag{5}$$

$$\times \frac{d^3 p_0}{(2\pi)^3 2E_0} \prod_x \frac{d^3 p_X}{(2\pi)^3 2E_X}.$$

But, for given m_A, m_B, p_A and p_B we can write:

$$d\sigma_0 = \frac{d^3 p_0}{2E_0} f(m_0, \vec{p}_0), \tag{6}$$

and the $f(m_0, \vec{p}_0)$ could be taken from the experimental data on stable particle subthreshold production [6]:

$$f(m_0, \vec{p}_0) = K \exp\left[-\frac{\sqrt{s_{\min}}}{\langle s_{\min}^{1/2}\rangle}\right]\left[0.9\exp(-2.7|\vec{p}_0|^2\sin^2\theta_0) + 0.1\right]. \quad (7)$$

We extended this general behaviour of the cross section (6) to unstable (resonance) particle production.

2. Particle Production and Decay Rate

Production rate of an unstable 0 particle in inclusive reaction (1) depends, besides the cross section, also on the overall decay rate term. As the process looks like:

$$x_A \cdot m_A + x_B \cdot m_B \to m_0 + M_X, \quad \text{(8)}$$
$$\qquad\qquad\qquad\qquad\qquad\qquad\quad \llcorner\!\!- - \to m_1 + m_2$$

then the production rate is:

$$\frac{dN_0}{dt} = \Phi_B \sigma_0 N_A - \Gamma N_0, \quad (9)$$

where: Φ_B is the flux density of the beam particles; σ_0, the inclusive cross section for the 0 particle production; N_A, the number of the A target particles; Γ, the decay probability in time unit, for the 0 particle. After a proper integration, the time asymptotically differential distribution of the 0 particle will be:

$$dN_0 = \frac{\Phi_B N_A}{\Gamma} d\sigma_0 . \quad (10)$$

The decay rate of the 0 particles into the final state element $d\vec{p}_1 \cdot d\vec{p}_2$ can be written by multiplying this dN_0 particle number with the transition probability [7]:

$$dR_{12} = \frac{1}{2E_0}|\mathfrak{M}_{0\to 1+2}|^2 (2\pi)^4 \sigma^4(p_0 - p_1 - p_2) \frac{d\vec{p}_1}{(2\pi)^3 2E_1} \frac{d\vec{p}_2}{(2\pi)^3 2E_2} dN_0, \quad (11)$$

$d\sigma_0$ in (10) is the differential cross section (6) and Γ is the decay probability in time unit to all possible momenta $\vec{p}_1$ and $\vec{p}_2$:

$$\Gamma = \frac{1}{2E_0}|\mathfrak{M}_{0\to 1+2}|^2 (2\pi)^4 \int \sigma^4(p_0 - p_1 - p_2) \frac{d\vec{p}_1}{(2\pi)^3 2E_1} \frac{d\vec{p}_2}{(2\pi)^3 2E_2} . \quad (12)$$

For unpolarized particle production, the $|\mathcal{M}_{0\to 1+2}|^2$ are constant, and the integral in (12) is the two-particle phase space one [8]:

$$\int \sigma^4(p_0 - p_1 - p_2)\frac{d\vec{p}_1}{(2\pi)^3 2E_1}\frac{d\vec{p}_2}{(2\pi)^3 2E_2} = \frac{|\vec{p}_1^*|\pi}{m_0}, \tag{13}$$

where: $|\vec{p}_1^*| = \sqrt{E_1^{*2} - m_1^2}$; $E_1^* = (m_0^2 + m_1^2 - m_2^2)/(2m_0)$.

If the m_0 mass distribution is taken as a Breit—Winger one:

$$\frac{1}{N_0}\frac{dN_0}{dm_0} = \frac{\Gamma/(2\pi)}{(m_0 - m_R)^2 + (\Gamma/2)^2}, \tag{14}$$

then the complete differential distribution of the decay rate into the final state element $d\vec{p}_1 \cdot d\vec{p}_2$ is given by (11), accounting also the (10), (6), (12), (13) and (14):

$$dR_{12} = \Phi_B N_A \frac{m_0}{|\vec{p}_1^*|\pi}\sigma^4(p_0 - p_1 - p_2)\frac{1}{N_0}\frac{dN_0}{dm_0}dm_0 \times$$

$$\times f(m_0, \vec{p}_0)\frac{d\vec{p}_0}{2E_0}\frac{d\vec{p}_1}{2E_1}\frac{d\vec{p}_2}{2E_2}. \tag{15}$$

3. The Final State Particle Distributions Due to ρ and J/ψ Subthreshold Production and Decay

The final state particle distribution, due to unstable particle production and decay, gives the necessary elements to design and arrange the experimental work. They show the spectral characteristics due to both kinematics of the process and its dynamics. So, it is possible to correlate the actior of different detection elements, to organize an efficient trigger system and to optimize the detector configuration for a given physical process study.

Any one of the possible distributions is done by integrating the dR_{12} element (15) over all the variables, except the one specifying the distribution itself, which is taken in constant steps on every surface, corresponding to constant values of this variable. The multiple integration, in this work, was carried out by Monte — Carlo method [9].

The simullated physical processes are an 8.9 GeV/c proton-nucleus interaction, followed by a 0 (ρ and J/ψ) particle production and decay.

The cross section is taken from the stable meson subthreshold production [6] and is extended to this vector meson production. We considered the two particle final states (pions from ρ meson decay and electrons from J/ψ meson decay) for integration over their phase space and sought the characteristic distributions.

The $\vec{p}_0$ momentum is taken as a constant vector, as long as m_0 takes Breit — Wigner distributed values. The final particle momentum vectors $\vec{p}_1$ and $\vec{p}_2$, are generated as two constant module opposite vectors $|\vec{p}^*|$, isotropically distributed in the CM system of the decaying particle, followed by a general Lorentz transformation to the laboratory system.

The most interesting distributions are presented in the Figures 1—11. Every one is based on 100,000 generated events. The lines on all the graphics are drawn by a spline fit procedure. In the next, we will analyze the ρ and J/ψ distributions. The main differences are due to the fact that the resonance width is large for ρ meson ($\Gamma =$ 153 MeV) and small for J/ψ meson ($\Gamma =$ 0.00472 MeV).

— The cross section changes strongly on the ρ mass interval, but on the J/ψ mass interval it is practically constant. Consequently, the two-pion *effective mass distribution*, from the ρ meson decay, (the same with its mass distribution), shows a strong cross section dependence especially in the low mass part (Fig.1), while the high mass part shows a Breit — Wigner behaviour.

By contrary, the two-electron effective mass distribution from the J/ψ decay has not any cross section influence, neither on the J/ψ mass nor on its momentum and angle values. It is the same with the Breit — Wigner distribution.

— The one-particle *energy distributions* for

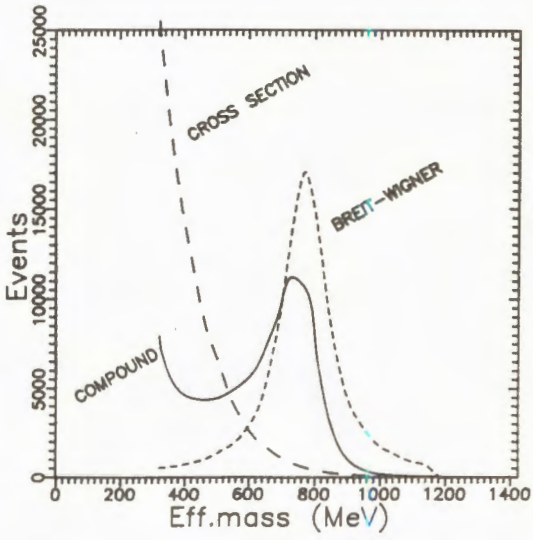

Fig.1. The two-pion effective mass distribution from the ρ meson decay for $p_\rho = 500$ MeV/c. The ρ meson production cross section mass dependence and Breit — Wigner mass distribution influence are plotted separately.

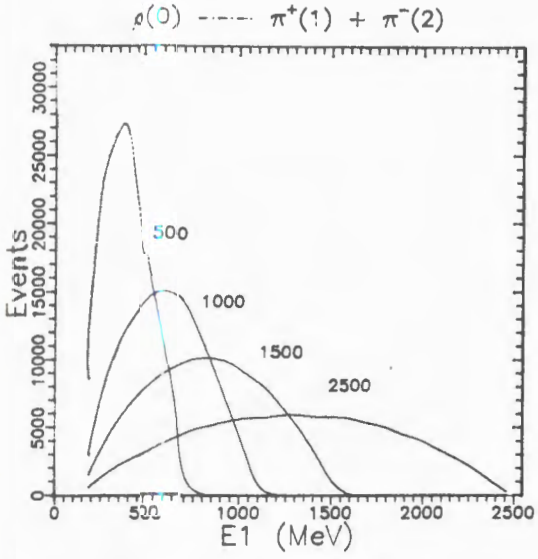

Fig.2. The one-pion energy distirubiton from the ρ meson decay for $p_0 = 500, 1000, 1500, 2500$ MeV/c.

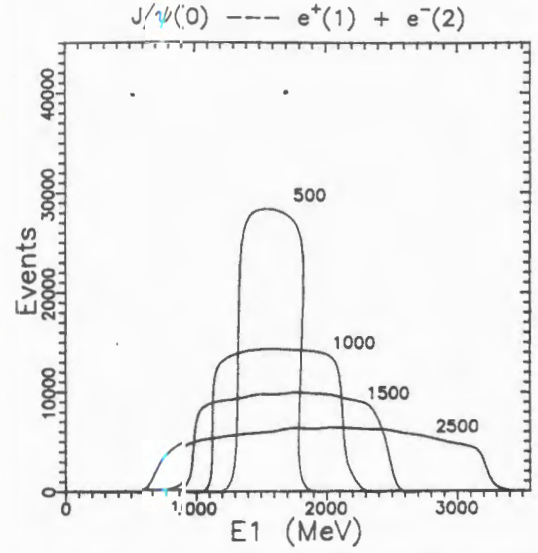

Fig.3. The one-electron energy distribution from the J/ψ meson decay for $p_{J/\psi} = 500, 1000, 1500, 2500$ MeV/c.

the ρ and J/ψ meson decay products are shown in Figs.2, 3. The dynamics (cross section) and Breit — Wigner affect the one-pion distribution from the ρ meson decay (Fig.2), modifying the pure kinematic to rectangular one. For the J/ψ decay, because the electron CM $\cos\theta_1^*$ has uniform distribution and the $\Gamma_{J/\psi} \approx 0$, the one-electron energy distribution in the laboratory system has also a uniform distribution, mainly a kinematic rectangular behaviour (Fig.3), between the limits:

$$E_1 = (E_1^* \cdot E_0 \pm |\vec{p}_1^*| \times$$

$$\times |\vec{p}_0| / m_0.$$

— The one-particle *angular distributions* for some meson momentum values are shown in Figs.4, 5. There can be seen a net particle flight, on the initial meson direction, especially evident for high momentum ρ meson. The J/ψ meson has a more flat angular distribution.

— The *opening angle distributions* of the two

particles from the ρ and J/ψ decay are presented in Figs.6, 7. For the two pions of the ρ meson decay, the opening angle distribution has a clear maximum for every ρ momentum values (Fig.6). For the two electrons of the J/ψ decay, the θ_{12} angle distribution shows a clear low limit, for every J/ψ energy value (Fig.7), in accordance with the well-known relation (when $m_1 = m_1 = m_2 \ll m_0$): $\theta_{12}^{\min} = -2 \arcsin (m_0/E_0)$.

— The last analyzed distribution is the one-particle *transverse momentum distribution* for the decay products of the ρ and J/ψ shown in Figs.8—11. Obviously, the distributions are very sensitive to the ρ and J/ψ meson emission angle θ_0. As long as $\theta_0 = 0°$, the one-particle transverse momentum distributions coincide for all the $\vec{p}_0$ values, while for $\theta_0 = 90°$ they show a strong momentum dependence (Figs.9,10). In the same time, the electron p_t distribution

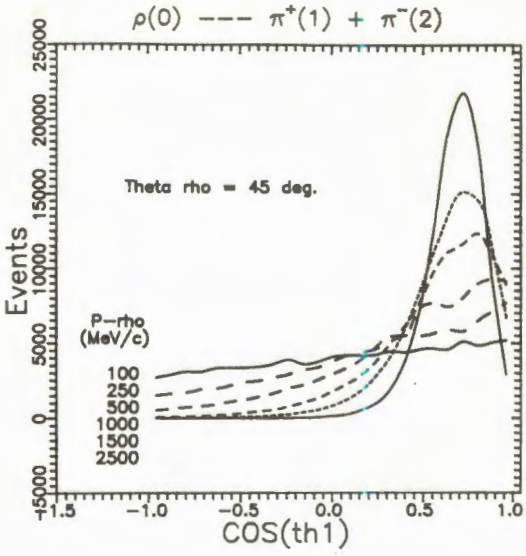

Fig.4. The one-pion angular distribution from the ρ meson decay, under $\theta_\rho = 45°$, for $p_\rho = 100$, 250, 500, 1000, 1500, 2500 MeV/c

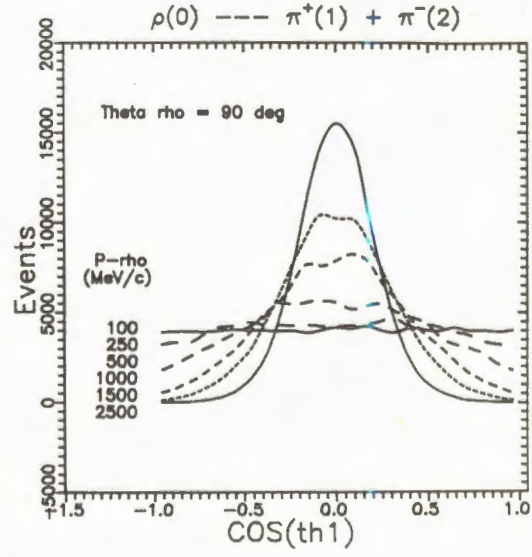

Fig.5. The one-pion angular distribution from the ρ meson decay, under $\theta_\rho = 90°$, for $p_\rho = 100$, 250, 500, 1000, 1500, 2500 MeV/c

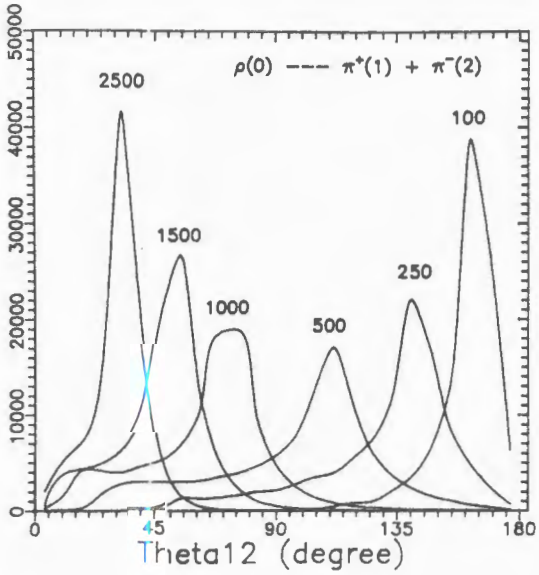

Fig.6. The relative flight angle distribution of the two pions from the ρ meson decay for p_ρ = 100, 250, 500, 1000, 1500, 2500 MeV/c

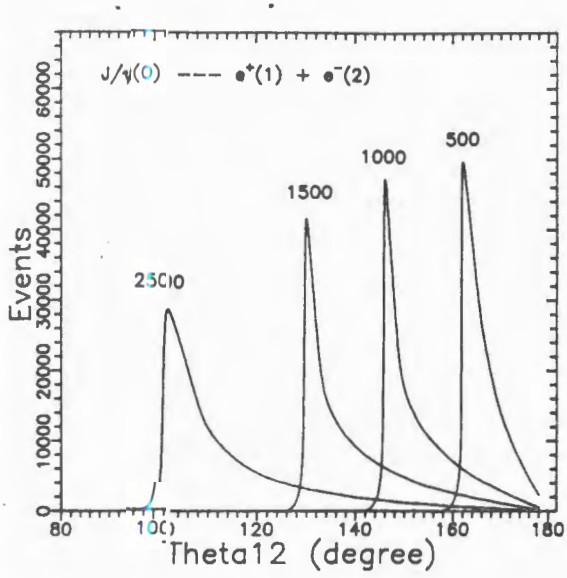

Fig.7. The relative flight angle distribution of the two electrons from the J/ψ meson decay for $p_{J/\psi}$ = 500, 1000, 1500, 2500 MeV/c

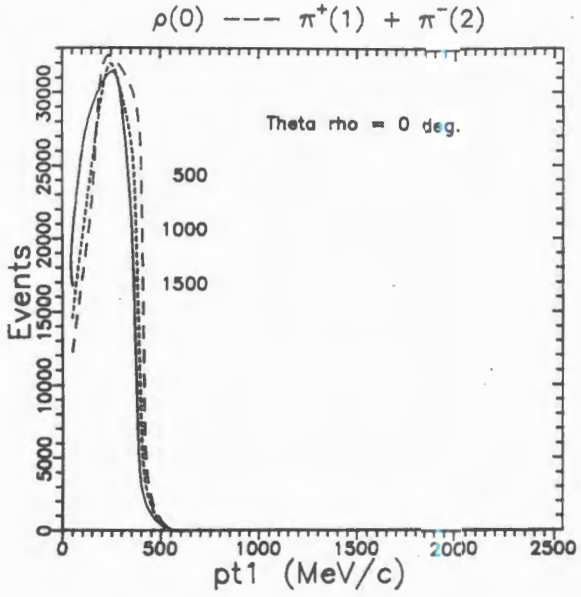

Fig.8. The one-pion transverse momentum distribution from the ρ meson decay, under $\theta_\rho = 0°$, for $p_\rho = 500$, 1000, 1500 MeV/c

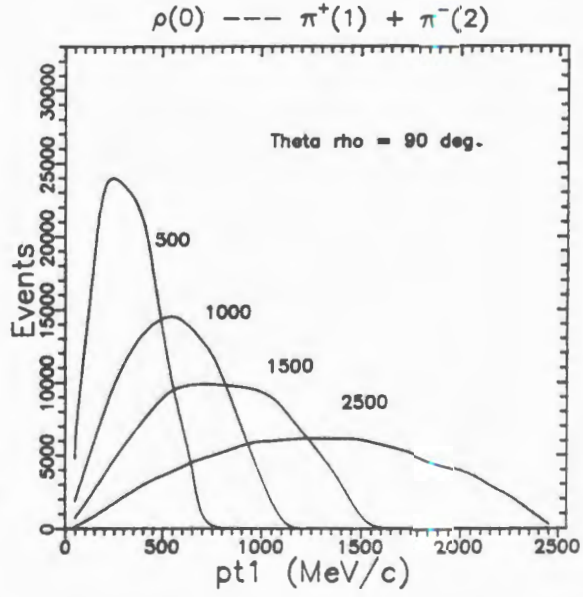

Fig.9. The one-pion transverse momentum distribution from the ρ meson decay, under $\theta_\rho = 90°$, for $p_\rho = 500$, 1000, 1500, 2500 MeV/c

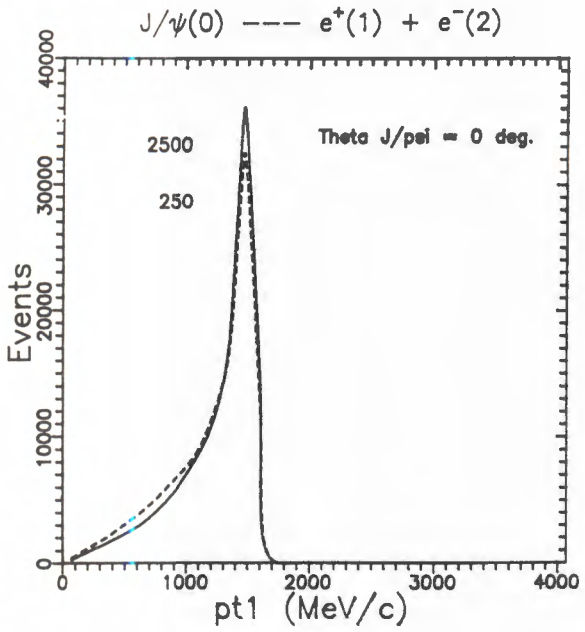

Fig.10. The one-electron transverse momentum distribution from the J/ψ meson decay, under $\theta_{J/\psi} = 0°$, for $p_{J/\psi} = 250$, 2500 MeV/c

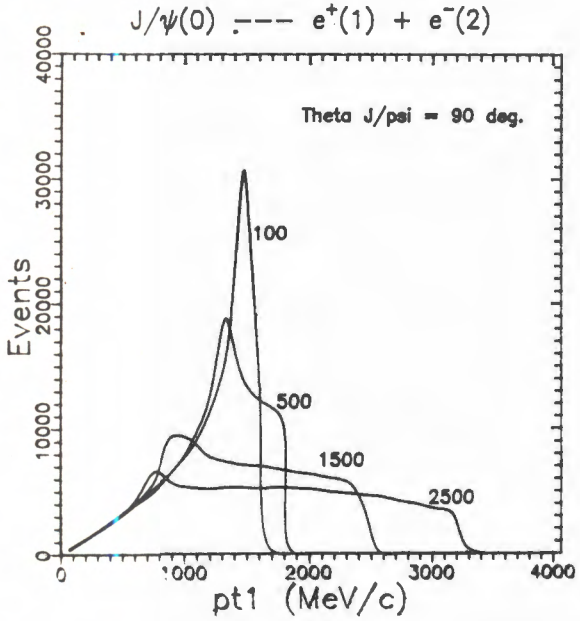

Fig.11. The one-electron transverse momentum distribution from the J/ψ meson decay, under $\theta_{J/\psi} = 90°$, for $p_{J/\psi} =$ 100, 500, 1500,

from the J/ψ decay for $\theta_0 = 0°$, shows a clear p_{t1}^{max} limit (Fig.10). If the cross section influence can be neglected, then the p_{t1}^{max} can be expressed, in the same $m_1 = m_2 << m_0$ approximation, as [10]: $p_{t1}^{max} = m_0/2$, and is independent of the J/ψ momentum (energy).

4. Conclusions

Phenomenological approach of the subthreshold production [6] was extended from the stable particle (pseudoscalar mesons, protons and antiprotons) to ρ and J/ψ vector meson production. Using the Monte — Carlo simulation and the final state phase space integration, we propose some particular distributions. Analyzing the characters, peculiarities and kinematical aspects of this distributions it is possible to prepare a proper experiment for the study of the ρ and J/ψ meson production in nuclear subthreshold interactions.

Acknowledgements. We wish to express special thanks to S.V.Afanasiev, V.V.Arkhipov, S.Reznikov and A.Yu.Semenov for computer assistance.

References

1. Baldin A.M. et al. — JINR, E1-8054, Dubna, 1974.
   Baldin A.M. et al. — JINR, E1-82-472, Dubna, 1982.
   Baldin A.M. et al. — JINR, P1-83-433, Dubna, 1983.
2. Gorenstein M.I., Zinovjev G.M. — Phys. Lett., 1977, 67B, p.100.
3. Berlad G., Dar A., Eilam G. — Phys. Rev. D, 1980, 27, p.1547.
4. Ghiordanescu N., Stavinsky V.S. — JINR, P2-81-369, Dubna, 1981.
5. Pentia M. et al. — St. Cerc. Fiz., t.37, N.6—8, p.740, Bucuresti, 1985, (in Romanian).
6. Stavinsky V.S. — Proceedings IX Int. Seminar on H.E.P.Problems, Relativistic Nucl. Phys. and Q.C.D., Dubna, 14—19 June, 1988, JINR D1,2-88-652, Dubna, 1988, p.190.
7. Halzen F., Martin A.D. — Quarks and Leptons, An Introductory Course in Modern Particle Physics, Wiley, New-York, 1984.
8. Kopylov G.I. — Osnovy Kinematiki Resonansov, Nauka, Moskva, 1970.
9. Sobolj I.M. — Chislennye Metody Monte-Carlo, Nauka, Moskva, 1973.
10. Goldansky V.I., Nikitin Yu.P., Rosental I.L. — Kinematicheskie Metody v Fizike Vysokikh Energij, Nauka, Moskva, 1987.

Received on July 7, 1992.